ELSEVIER

Journal of Nuclear Materials 294 (2001) 123–129

journal of nuclear materials

www.elsevier.nl/locate/jnucmat

Thermodynamic evaluation of the quaternary U–Pu–Zr–Fe system – assessment of cladding temperature limits of metallic fuel in a fast reactor

Masaki Kurata *, Kinya Nakamura, Takanari Ogata

Central Research Institute of Electric Power Industry, Iwado-kita 2-11-1, Komae-shi, Tokyo, 201-8511, Japan

Abstract

The quaternary U–Pu–Zr–Fe system was assessed using thermodynamic and phase diagram data in order to evaluate fuel-cladding chemical interactions (FCCI) of metallic fuel in a fast reactor. The Gibbs energy of mixing for solution phases and the Gibbs energy of formation of compounds in the binary sub-systems were calculated using an optimization procedure. The use of such data in optimizing the binary sub-systems enabled appropriate calculations for the thermodynamic properties of the systems, which were also important when extrapolating to higher-order systems. Isotherms of ternary sub-systems were calculated by using the optimized parameters of the binary sub-systems. Based on the phase relation data measured in regions of the ternary systems, the isotherms were then modified by adding ternary interaction parameters. The calculation results agreed well with the experimental data points. Finally, the quaternary system was assessed. The phase relationship observed experimentally in the diffusion couple of U–Pu–Zr–Fe was in reasonable agreement with the calculated phase diagrams.

1. Introduction

U–Pu–Zr alloys have been recognized as excellent candidates for advanced fast reactor fuels because of their high burnup capability, favorable thermal response, inherent safety, and excellent compatibility with pyro-reprocessing. The evaluation of fuel-cladding chemical interaction (FCCI) is important in the assessment of cladding temperature limits for the use of metallic fuels in fast reactors [1]. In the present study, the quaternary U–Pu–Zr–Fe system was assessed to provide basic data for the evaluation of FCCI. First, it was necessary to obtain thermodynamic data for the six binary sub-systems, such as the Gibbs energy of mixing of solution phases and the Gibbs energy of formation of compounds [2–4]. In these latter references thermodynamic data and phase diagram information were used in the optimizations. Accurate thermodynamic data for the binary sub-systems was very important when extrapolating to higher-order systems. A preliminary thermodynamic assessment was carried out for the Fe–Pu system in the present study, although the experimental data are limited. Next isotherms of the ternary sub-systems were calculated by using the optimized parameters for the binary sub-systems. The assessments of the U–Pu–Zr and Fe–U–Zr sub-systems were carried out in the previous study [2,4]. In the present study, the assessment of the Fe–Pu–U ternary system was attempted and since no experimental data were available, annealing tests were also performed. The preliminary data for the Fe–Pu–U system were then modified based on the experimental results. The parameters for the Fe–Pu–U system optimized in the present study are shown in the appendix. Finally, the quaternary system was assessed. The phase relationship observed experimentally in the diffusion couple of U–Pu–Zr–Fe reported previously [5] was in reasonable agreement with the calculated quaternary phase diagram.

* Corresponding author. Tel.: +81-33 480 2111; fax: +81-33 480 7956.

E-mail address: kurata@criepi.denken.or.jp (M. Kurata).

0022-3115/01/$ - see front matter
PII: S0022-3115(01)00473-1

2. Experimental study on Fe–Pu–U system

2.1. Procedure

Seven specimens of Fe–Pu–U alloy were prepared by arc-melting on a water-cooled copper hearth in a purified argon atmosphere. The purities of iron and uranium ingots before melting were 99.9% and 99.995%, respectively. The plutonium ingots contained approximately 1.4% of americium as impurity. The seven specimens were individually wrapped with tungsten foil and individually encapsulated in stainless steel cans under an atmosphere of argon. They were then annealed at 923 K for 1 week. After annealing, the capsules were quenched by dropping into an oil bath. The annealed specimens were cut into two parts and the cut surface of one part was ground and polished for electron probe microanalysis. The compositions of various phases were measured by SEM–EDX with ZAF correction. The other part of each specimen was dissolved in nitric acid and the compositions were measured by chemical analysis, the results are listed in Table 1.

2.2. Experimental results

Fig. 1 shows back-scattered electron images of the annealed samples. Two phases are observed in all the samples except for no. 4. Although grey and black regions are seen in sample no. 4, the grey region contained two phases, Pu-rich liquid and $Fe(Pu,U)_6$, which could not be distinguished by SEM. The measured compositions of various phases are summarized in Table 2. Samples nos. 1, 2, 3, and 4 have a phase in which the mole ratio of Fe to the sum of U and Pu is approximately 1–6. In contrast, samples nos. 3, 4, 5, 6, and 7 have another phase in which the mole ratio is approximately 2 to 1. According to the published binary phase diagrams [6], two kinds of compounds with the mole ratio of 1:6 and 2:1 exist in the Fe–U and Fe–Pu systems. These facts suggest that there are mutual solubilities between the Fe–U and Fe–Pu compounds in the Fe–Pu–U system. In sample no. 4, $Fe(Pu,U)_6$ and Fe_2 (Pu,U) were detected by EDX. The composition of the liquid phase could not be determined because the size of each liquid phase region was smaller than 5 μm and was not homogeneous due to segregation during solidification. Since the size of the liquid phase region was much larger in samples nos. 5, 6, and 7, the composition could be determined by area scan measurements using EDX. The tie-lines for the sample compositions, with the exception of sample no. 4, were determined from these measurements. In the case of sample no. 4 the compositions of the phases $Fe(Pu,U)_6$ and Fe_2 (Pu,U), that formed the three-phase region, were also derived.

Table 1
Initial composition of annealed samples

Sample no.	Composition analyzed (at.%)		
	Fe	Pu	U
1	10.08	24.54	65.38
2	6.39	17.53	76.08
3	34.88	4.64	60.48
4	22.01	22.31	55.69
5	50.39	29.46	20.15
6	35.34	25.66	39.00
7	41.03	58.97	0.00

3. Thermodynamic calculations

3.1. Thermodynamic models

The pure solid elements at 298.15 K in their stable form were chosen as the reference state of the system. For the thermodynamic functions of the pure elements in their stable states, the Scientific Group Thermodata Europe (SGTE) phase stability equations were used [7]. The equations are given in the form

$$ {}^0G_i^{\phi}(T) - H_i^{\phi} = a + bT + cT\ln T + dT^2 + eT^{-1} + fT^3 + iT^7 + jT^{-9} \quad (1) $$

as a function of temperature, where the stability of ϕ-phase is described relative to the stable element reference (SER) at 298.15 K.

The liquid, bcc, and fcc phases were modeled as substitutional solutions in the Fe–Pu–U ternary system. The α-U, β-U, β-Pu, γ-Pu, and δ′-Pu phases as well as the intermediate η- and ζ-phases were modeled as substitutional solutions in the Pu–U binary system [4]. The Gibbs energy for these solution phases is described by the approximation expressed as follows:

$$ G_{\mathrm{mix}}^{\phi} = x_i\,{}^0G_i^{\phi} + x_j\,{}^0G_j^{\phi} + RT(x_i\ln x_i + x_j\ln x_j) + x_ix_jL_{i,j}^{\phi}, \quad (2) $$

where i and j indicate elements, and ${}^0G_i^{\phi}$ and ${}^0G_j^{\phi}$ are the molar Gibbs energies of pure i and j as the ϕ-phase with respect to SER. The interaction parameters in Eq. (2), $L_{i,j}^{\phi}$, are defined with a Redlich–Kister polynomial as follows:

$$ L_{i,j}^{\phi} = x_ix_j[L^{\phi,0} + (x_i - x_j)L^{\phi,1} + (x_i - x_j)^2L^{\phi,2}]. \quad (3) $$

The intermetallic compounds are, on the other hand, treated as line compounds.

The ternary systems are modeled in a similar manner as follows:

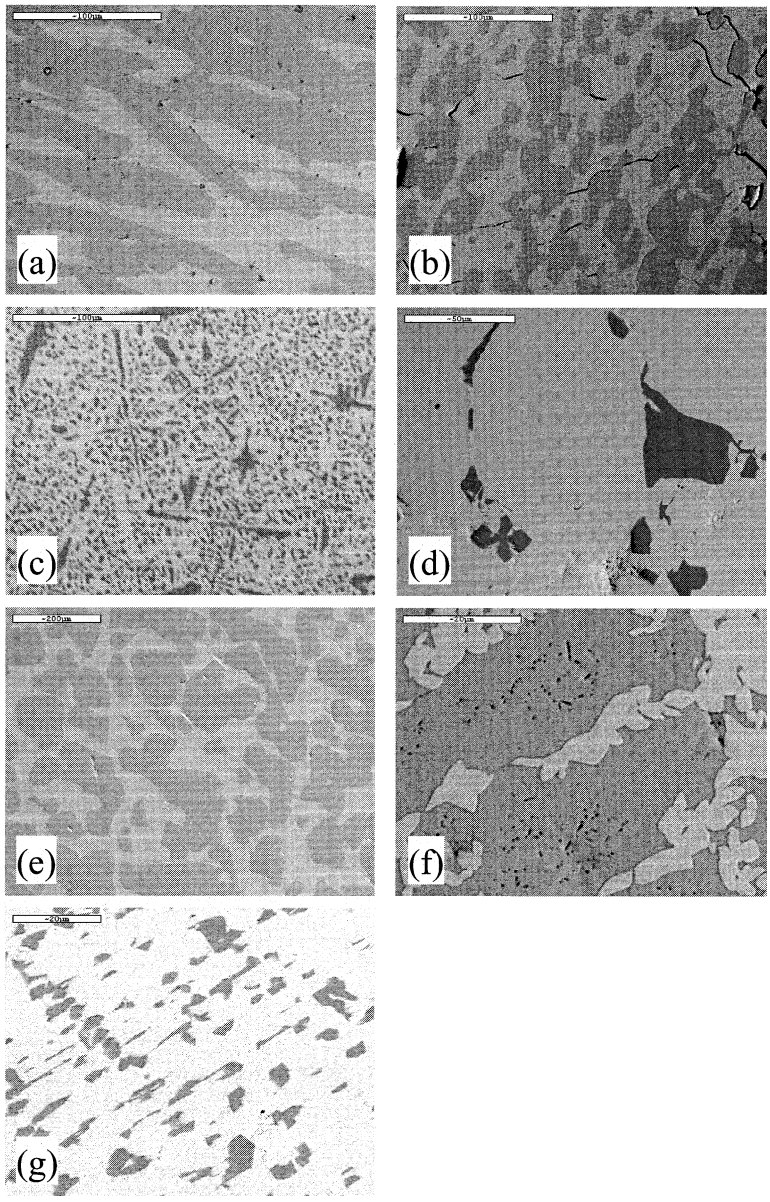

Fig. 1. BSE image of annealed samples. (a) no. 1, (b) no. 2, (c) no. 3, (d) no. 4, (e) no. 5, (f) no. 6 and (g) no. 7.

$$G^{\phi}_{\mathrm{mix}} = x_i{}^0G^{\phi}_i + x_j{}^0G^{\phi}_j + x_k{}^0G^{\phi}_k + RT(x_i \ln x_i + x_j \ln x_j + x_k \ln x_k) + x_ix_jL^{\phi}_{i,j} + x_jx_kL^{\phi}_{j,k} + x_kx_iL^{\phi}_{k,i} + x_ix_jx_kL_{i,j},k^{\phi}. \quad (4)$$

In modeling the ternary system, G^{ϕ}_{mix} is estimated initially without adding any ternary parameters. This preliminary estimation for the U–Pu–Fe system, based on the binary parameters, was then modified by taking into account the experimental data given in Section 2. The quaternary system U–Pu–Zr–Fe was finally estimated based on the data for the ternary sub-systems.

4. Calculated results and discussion

4.1. Fe–Pu system

Although the data for the Fe–Pu phase diagram were given in Refs. [8,9], the experimental results were rather limited. The Fe_2Pu and $FePu_6$ compounds exist, analogous to the Fe_2U and FeU_6 compounds in the Fe–U system. The former compound decomposes congruently and the latter peritectically. A phase transformation for Fe_2Pu was observed at approximately 1300 K. In the

Table 2
Composition of each phase in annealed samples

Sample no.	Composition analyzed (at.%)			Phase predicted from analysis
	Fe	Pu	U	
1	13.7	16.4	69.9	$Fe(Pu, U)_6$
	0.7	36.1	63.2	η-(Pu, U)
2	12.3	11.7	76.0	$Fe(Pu, U)_6$
	0.2	23.4	76.5	β-U
3	65.3	0.9	69.9	$Fe_2(Pu, U)$
	15.3	6.1	78.6	$Fe(Pu, U)_6$
	64.6	3.3	32.1	$Fe_2(Pu, U)$
4	13.3	14.3	72.4	$Fe(Pu, U)_6$
	–	–	–	Liquid[a]
	63.5	9.2	27.3	$Fe_2(Pu, U)$
5	20.7	70.2	9.1	Liquid
	66.3	4.5	29.2	$Fe_2(Pu, U)$
6	16.1	37.9	45.9	Liquid
	61.9	38.1	–	$Fe_2(Pu, U)$
7	17.8	82.2	–	Liquid

[a] The composition of the liquid phase in sample no. 4 could not be measured, because it had not solidified homogeneously.

present study, a preliminary least square calculation was performed using the equilibrium at the invariant temperatures in the Fe–Pu system, and the initial values of the interaction parameters were obtained. These were then optimized with the PARROT module of the Thermocalc code [10]. Since there is insufficient data, the phase transformation for Fe_2Pu is neglected in the calculation. Fig. 2 shows the calculated phase diagram together with the experimental data; there is reasonable agreement between the two with the exception of the Pu-rich region at low temperature. The derived parameters are listed in Appendix A.

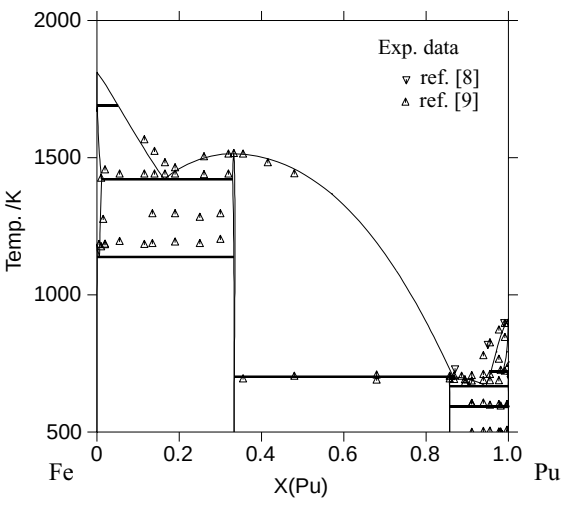

Fig. 2. Calculated Fe–Pu phase diagram.

4.2. Fe–Pu–U system

Fig. 3 shows the preliminary estimation of the Fe–Pu–U isotherm at 923 K, assuming that the two isostructural compounds of Fe–Pu and Fe–U form an ideal solution across the composition range. The experimental results described in Section 2 are also plotted in the same figure. The calculated tie-lines show a similar tendency to the experimental ones. Slight differences in composition are found in the equilibrium between the liquid and FeU_6 phases. The experimental solubility of Pu in FeU_6 is approximately 16 at.%, slightly higher

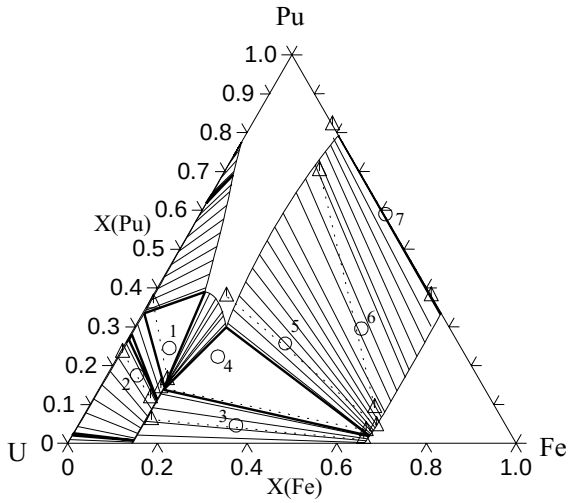

Fig. 3. Calculated Fe–Pu–U isotherm at 923 K based only on binary parameters. (○) Initial composition, (△ · · · △) detected tie-line.

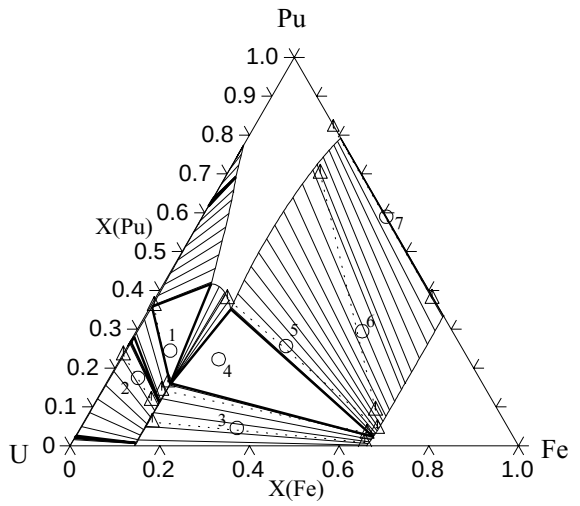

Fig. 4. Calculated Fe–Pu–U isotherm at 923 K after introducing ternary parameter to liquid phase. (○) Initial composition, (△ · · · △) detected tie-line.

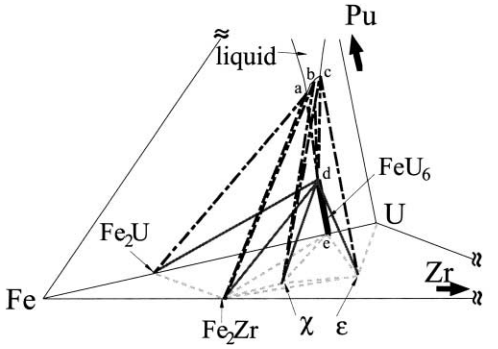

Fig. 5. Quaternary U–Pu–Zr–Fe phase diagram for the region rich in Fe and U at 923 K. (⋯⋯) phase boundaries of three phase region in U–Zr–Fe sub-system, (——) phase boundries of three phase tetrahedra containing FeU_6 in U–Pu–Zr–Fe system, (——— ⋯ ———) phase boundaries of four phase tetrahedra containing FeU_6 and liquid in U–Pu–Zr–Fe system.

than the calculated value. The calculation was modified by adding a ternary interaction parameter to the liquid phase for the following reasons. In the modeling of the Fe–U binary system, the Gibbs energy for the liquid phase is optimized using the data reported for the temperature region above 998 K. The value obtained is, therefore, extrapolated in the modeling of the Fe–Pu–U ternary system at lower temperatures. Consequently, it may cause larger error than the other parameters. Furthermore, the calculated tie-lines between FeU_6 and β-U or η in Fig. 3 almost coincide with the experimental data, indicating that the estimation of the Gibbs energy of FeU_6 is reasonable. Hence the data for the liquid phase should be modified to increase the Pu-solubility in the FeU_6 compound as determined in the experimental study. The value of $L_{i,j}, k^{\text{liquid}}$ is estimated to be +10 kJ/mol by trial and error. Fig. 4 shows the modified U–Pu–Fe isotherm, which is in better agreement with the experimental data. As mentioned in Section 2.2, the liquid phase composition in the $Fe(Pu,U)_6$–Fe_2 (Pu,U)-liquid three-phase region was not determined experimentally. The calculated value for this composition almost coincides with the liquid phase composition determined in sample no. 5. Further experiments are, however, required to determine an accurate value.

4.3. U–Pu–Zr–Fe system

Considering the FCCI interaction, the region rich in Fe and U in the U–Pu–Zr–Fe system is the most important, especially the composition where liquid phase exists. Although a quaternary phase diagram is drawn as a tetrahedron, Fig. 5 shows a section of the region rich in Fe and U at 923 K. The figure is drawn without any quaternary parameters. The base corresponds to the Fe–U–Zr sub-system and the left-back side to the Fe–Pu–U sub-system. The grey dotted lines on the base indicate the phase boundaries of three-phase region in the Fe–U–Zr sub-system. A thick solid line on the left-back side shows the FeU_6 type phase and point marked d corresponds to the solubility limit of Pu in the FeU_6 phase. FeU_6 is very stable at 923 K and is in equilibrium with Fe_2U, Fe_2Zr, χ, and ε-phases by forming tetrahedra containing three phases, indicated as d-e-χ-ε, d-e-χ-Fe_2Zr, and d-e-Fe_2Zr–Fe_2U in the figure. The χ and ε phases were the ternary compounds in the U–Zr–Fe system found in our previous study [11]. The grey solid lines show the upper phase boundaries of these tetrahedra. In the upper region of these three-phase tetrahedra, there are several four-phase tetrahedra containing both FeU_6 and liquid, indicated as c-d-χ-ε, b-d-χ-Fe_2Zr, and a-d-Fe_2Zr–Fe_2U. Between these four-phase tetrahedra, three-phase regions should exist which include liquid phase.

Ogata et al. carried out diffusion tests at 923 K using U–Pu–Zr–Fe couples with two different Pu concentrations [5]. The apparent diffusion paths observed in their work are shown in Fig. 6, which is an enlargement of a section of Fig. 5, as thick dotted grey and black lines, labeled D1 and D2. The compositions of D1 and D2 are 64U–13Pu–23Zr and 55U–22Pu–23Zr in at.%, respectively. The liquid phase was only formed in D2. The diffusion path observed in D2 apparently exists on the surface of the liquid-containing four-phase tetrahedra in the calculated diagram. In contrast, the liquid phase was not observed in D1, which passes through the three-phase tetrahedra in the calculated diagram. In other words, the experimental observation and calculated diagram are consistent. These observations lead to the conclusion that liquid phase must be formed in a U–Pu–

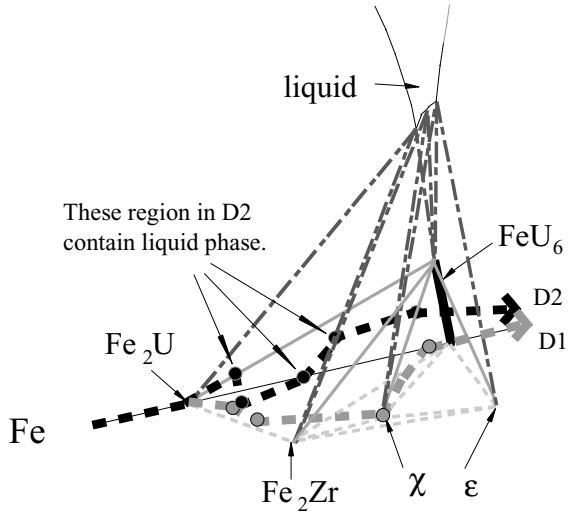

Fig. 6. Enlargement of tetrahedra containing liquid phase and diffusion path observed in U–Pu–Zr–Fe couple at 923 K in the previous study [5]. (■■■) diffusion path observed in 55U–22Pu–23Zr–Fe couple (D2), (▩▩▩) diffusion path observed in 64U–13Pu–23Zr–Fe couple (D1), (▒ ●) average composition of various layers observed in diffusion paths.

Zr–Fe diffusion couple at 923 K under the condition that a diffusion path between U–Pu–Zr fuel and Fe cladding exists on the surface of the four-phase tetrahedra.

5. Conclusion

A thermodynamic assessment was carried out to investigate the phase relationships in the U–Pu–Zr–Fe system. First, the Fe–Pu system was assessed. By combining the calculated parameters for the Fe–Pu system with the previously calculated parameters for the Fe–U and Pu–U systems, a reasonable representation of the Fe–Pu–U system was obtained without introducing any ternary parameters. The Fe–Pu–U model was then slightly modified by adding a ternary parameter to the liquid phase, based on annealing test results. A four-phase region, containing liquid, of the U–Pu–Zr–Fe system was considered in order to understand the liquid formation mechanism in the diffusion couple of U–Pu–Zr fuel and cladding at 923 K. The phase relationship observed experimentally in the diffusion couple was in reasonable agreement with the calculated phase diagrams.

Acknowledgements

The authors are grateful to M.A. Mignanelli of AEA Technology for his great help in the experimental study on the Fe–Pu–U system and to T. Yokoo of CRIEPI for his useful suggestions on the FCCI mechanism. The authors would also like to express their many thanks to I. Ansara and C. Servant of LTPCM for access to the Fe–Zr database.

Appendix A

The assessed parameters for the Fe–Pu–U system are shown as follows. The Gibbs energies for pure substances are given in the SGTE database [7]. The parameters for the Pu–U–Zr and Fe–U–Zr systems are given in the previous works [2,4]. The energies are given in joules per mole.

Phase: liquid.

$${}^{0}L^{\text{liquid}}_{\text{Fe,Pu}} = +28\,000 - 48.22\ \text{T},$$

$${}^{1}L^{\text{liquid}}_{\text{Fe,Pu}} = +21\,080,$$

$${}^{2}L^{\text{liquid}}_{\text{Fe,Pu}} = -16\,630,$$

$${}^{0}L^{\text{liquid}}_{\text{Fe,U}} = -34\,330 - 7.198\ \text{T},$$

$${}^{1}L^{\text{liquid}}_{\text{Fe,U}} = -8320,$$

$${}^{2}L^{\text{liquid}}_{\text{Fe,U}} = +6217,$$

$${}^{0}L^{\text{liquid}}_{\text{Pu,U}} = +4752 - 12.00\ \text{T},$$

$${}^{1}L^{\text{liquid}}_{\text{Pu,U}} = -2284,$$

$${}^{0}L^{\text{liquid}}_{\text{Fe,Pu,U}} = +10\,000.$$

Phase: bcc

$${}^{0}L^{\text{bcc}}_{\text{Fe,Pu}} = +20\,000,$$

$${}^{1}L^{\text{bcc}}_{\text{Fe,U}} = +1262,$$

$${}^{0}L^{\text{bcc}}_{\text{Pu,U}} = -5062,$$

$${}^{1}L^{\text{bcc}}_{\text{Pu,U}} = +506.8.$$

Phase: fcc

$${}^{0}L^{\text{fcc}}_{\text{Fe,Pu}} = +5000,$$

$${}^{0}L^{\text{fcc}}_{\text{Fe,U}} = -905.9,$$

$${}^{0}L^{\text{fcc}}_{\text{Pu,U}} = +3620.$$

Phase: Fe_2 (Pu,U)

$$G^{\text{Fe}_2(\text{Pu,U})}_{\text{Fe:Pu}} - 2.0{}^{\circ}H^{\text{liquid,298.15 K}}_{\text{Fe}} - 1.0{}^{\circ}H^{\text{liquid,298.15 K}}_{\text{Pu}} = -55\,130 + 3.038\ \text{T},$$

$$G^{\text{Fe}_2(\text{Pu,U})}_{\text{Fe:U}} - 2.0{}^{\circ}H^{\text{liquid,298.15 K}}_{\text{Fe}} - 1.0{}^{\circ}\text{H}^{\text{liquid,298.15 K}}_{\text{U}} = -90\,240 + 23.17\ \text{T},$$

$${}^{0}L^{\text{Fe}_2(\text{Pu,U})}_{\text{Fe:Pu,U}} = +0.$$

Phase: $Fe(Pu,U)_6$

$$G^{Fe(Pu,U)_6}_{Fe:Pu} - 1.0°H^{liquid,298.15\ K}_{Fe} - 6.0°H^{liquid,298.15\ K}_{Pu} = -161\,300 + 170.4\ T,$$

$$G^{Fe(Pu,U)_6}_{Fe:U} - 1.0°H^{liquid,298.15\ K}_{Fe} - 6.0°H^{liquid,298.15\ K}_{U} = -149\,400 + 87.76\ T,$$

$${}^0L^{Fe(Pu,U)_6}_{Fe:Pu,U} = +0.$$

References

[1] T. Ogata, PhD thesis, Kyoto University, Kyoto, 2000.
[2] M. Kurata, T. Ogata, K. Nakamura, T. Ogawa, J. Alloys Comp. 271–273 (1998) 636.
[3] C. Servant, C. Gueneau, I. Ansara, J. Alloys Comp. 220 (1995) 19.
[4] M. Kurata, CALPHAD 23 (1999) 305.
[5] T. Ogata, K. Nakamura, M. Kurata, T. Yokoo, M.A. Mignanelli, J. Nucl. Sci. Technol. 37 (2000) 244.
[6] T.B. Massalski, Binary Alloy Phase Diagrams, 2nd Ed., ASM International, 1990.
[7] A.T. Dinsdale, CALPHAD 15 (1991) 317.
[8] P.G. Mardon, M.A. Haines, J.H. Pearce, M.B. Waldron, J. Inst. Met. 86 (1957) 166.
[9] D. Ofte, L.J. Wittenberg, Trans. ASM 57 (1964) 916.
[10] B. Sundman, B. Jansson, J.-O. Andersson, CALPHAD 2 (1985) 153.
[11] K. Nakamura, M. Kurata, T. Ogata, A. Itoh, M. Akabori, J. Nucl. Mater. 275 (1999) 151.